


Tight-Binding Analysis of Excitonic States in Low-Dimensional GeSn Heterostructures

1st Alan Abdi 

Chair for Communication Technology
TU Dortmund
Dortmund, Germany
alan.abdi@tu-dortmund.de

2nd Tim Alexewicz

Chair for Communication Technology
TU Dortmund
Dortmund, Germany
tim.alexewicz@tu-dortmund.de

3rd Dirk Schulz 

Chair for Communication Technology
TU Dortmund
Dortmund, Germany
dirk2.schulz@tu-dortmund.de

Abstract—GeSn alloys have emerged as a promising material platform for Si-compatible optoelectronics, enabling efficient light emission and detection in the mid-infrared range due to their tunable direct band gap at high Sn concentrations. In our study, GeSn quantum well structures are modeled, focusing on how excitons govern the optical response of these nanostructures. Both short-range (on-site) and long-range (non-local) Coulomb effects are considered in the tight-binding excitonic Hamiltonian to assess their impact on the spectrum. The use of a density matrix in a real-space formulation allows for flexible inclusion of spatially dependent interactions. We systematically analyze the influence of varying Sn concentrations and investigate field-induced modifications of the excitonic states under externally applied electric fields. These parameters are shown to significantly affect the exciton binding energies and absorption spectra, including shifts in resonance energies and changes in oscillator strength.

Index Terms—Excitons, Tight-Binding, Density Matrix, GeSn Heterostructures

I. INTRODUCTION

Incorporating Sn into a Ge lattice reduces the Γ -point gap, with the band structure transforming from indirect to direct at Sn compositions above $\sim 8\%$. This transition makes GeSn promising for photonic applications, including optically and electrically driven GeSn lasers and integrated mid-infrared imaging in Si-based systems. The material's compatibility with epitaxial growth on Si substrates enables CMOS-integrated optoelectronic devices without the need for complex bonding techniques [1]. In this work, we analyze a quantum well composed of GeSn with different proportions of Sn, forming a heterostructure as shown in Fig. 1.

We focus on a stationary formulation of the excitonic problem, where the total two-particle Hamiltonian includes the band-edge potentials of the materials and the Coulomb interaction. The latter is considered in two limiting cases: a purely local interaction resembling the spinless Hubbard model used in [2], and a non-local interaction extending over multiple lattice sites. This comparison helps to reveal how the spatial range of the Coulomb potential affects exciton formation and energy levels. The system is built on the tight-binding (TB) approach outlined in [3] by extending the model, introducing two-particle correlations and tight-binding states as in [4], [5], with the numerical framework completed by

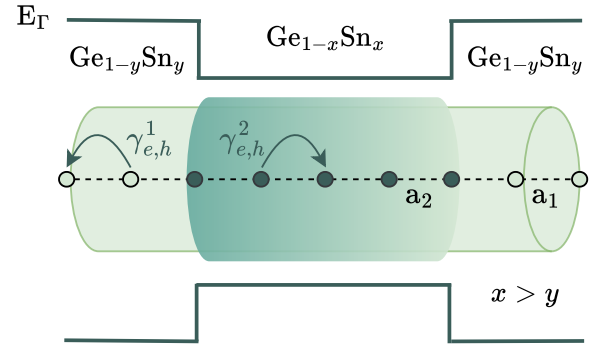


Fig. 1: Schematic illustration of the band edge profile E_Γ along the growth direction of a GeSn quantum well structure. For simplicity in the tight-binding modeling, identical hopping parameters $\gamma_{e,h}^1 = \gamma_{e,h}^2$ and uniform lattice spacing $a_1 = a_2$ were assumed, as both the lattice constant and effective masses vary only marginally with Sn composition.

incorporating the Coulomb interaction. The tight-binding formalism offers several advantages for modeling nanostructures such as quantum wells. Firstly, it naturally incorporates the atomistic lattice structure, allowing for an intuitive representation of quantum confinement and band mixing effects at the nanoscale. Secondly, the resulting Hamiltonians are sparse and efficiently diagonalizable, which is particularly beneficial for simulations involving large basis or multiple coupled particles, as in the case of excitonic systems. Moreover, site-dependent parameters enable straightforward incorporation of heterostructure potentials, electric fields, or interface effects, making the TB approach highly versatile for inhomogeneous systems.

Our TB model offers insight into the physical nature of bound exciton states in GeSn heterostructures. The formulation in terms of a density matrix further supports extensions toward time-dependent or dissipative effects, although the present study remains stationary. The model has been validated against reference data from literature, showing good agreement for exciton binding energies in both AlGaAs and GeSn material systems [6].

II. CONCEPT

We model the excitonic system using a real-space tight-binding framework for quantum wells by defining electron-hole pair states $|\phi_n, \phi_m\rangle$ as the direct product of the single-electron state $|\phi_n\rangle$ and the single-hole state $|\phi_m\rangle$ spanning an orthogonal basis

$$|\Psi_{ex}\rangle = \sum_{n,m} \hat{c}_n^\dagger \hat{d}_m^\dagger |\phi_n, \phi_m\rangle \quad (1)$$

with \hat{c}_n^\dagger being the creation operator for electrons and \hat{d}_m^\dagger for holes, respectively. The total Hamiltonian for the electron-hole pair then reads as

$$\hat{H}_{ex}^{tb} = \hat{H}_c^{tb} + \hat{H}_v^{tb} + V_e(n) - V_h(m) + V_c(n, m), \quad (2)$$

where:

- $\hat{H}_{c(v)}$ is the conduction (valence) band kinetic energy operator for electrons (holes),
- $V_e(n)$ and $V_h(m)$ are the spatially dependent confinement potentials,
- $V_c(n, m)$ represents the Coulomb interaction between electron and hole.

The kinetic energy operators are implemented using a nearest-neighbor coupling, following the approach in [3]. For notational simplicity, we adopt the convention $|\phi_n\rangle \equiv |n\rangle$, representing localized states directly by their site indices. Hence, for electrons, the tight-binding Hamiltonian reads

$$\hat{H}_c^{tb} = \sum_n \epsilon_n |n\rangle \langle n| + \gamma_e \sum_n |n\rangle \langle n+1| + \text{h.c.} \quad (3)$$

By exploiting the orthonormality of the localized basis states $|n\rangle$, the matrix representation of the tight-binding Hamiltonian \hat{H}_c^{tb} can be constructed by evaluating the matrix elements $\langle k | \hat{H}_c^{tb} | n \rangle$. This yields a sparse tridiagonal matrix structure, where the diagonal elements correspond to the on-site energies and the off-diagonal elements represent the coupling between neighboring lattice sites. Explicitly, we obtain:

$$\langle k | \hat{H}_c^{tb} | n \rangle = \epsilon_n \delta_{kn} + \gamma_e \delta_{k, n+1} + \gamma_e \delta_{k, n-1} \quad (4)$$

An analogous expression holds for the hole contribution \hat{H}_v^{tb} with corresponding hopping parameter γ_h .

In our model, the TB formalism serves as the foundation for constructing the full two-particle Hamiltonian in the tensor-product basis $|n, m\rangle = |n\rangle_e \otimes |m\rangle_h$, which captures the joint dynamics of electrons and holes. This enables the inclusion of both kinetic and interaction terms in a unified, real-space framework.

With the tensor-product basis in place, the full excitonic problem is formulated by solving the Schrödinger equation for the two-particle wavefunction $\Psi_{ex}(z_e, z_h)$, allowing a direct implementation of both single-particle and interaction terms in the discrete real-space representation:

$$\hat{H}_{ex}^{tb} \Psi_{ex}(z_e, z_h) = E \Psi_{ex}(z_e, z_h) \quad (5)$$

The variables z_e and z_h denote the spatial positions of the electron and hole, respectively, and are defined on a discrete

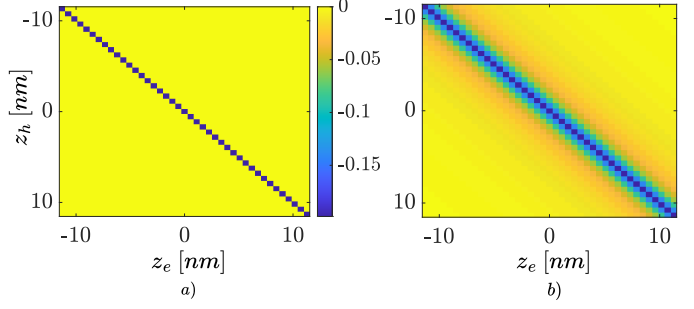


Fig. 2: Matrix representation of the Coulomb interaction $V_c(z_e, z_h)$. Left: Only diagonal matrix elements are included, corresponding to a purely short-range interaction. Right: Full long-range Coulomb interaction is implemented, regularized at zero separation by a small constant δ_r to avoid divergence.

spatial grid via $z_{e,h} = z_n = na$, where a is the lattice constant. This allows the tight-binding wavefunction $\Psi_{ex}(z_e, z_h)$ to be interpreted as a discretized representation of the continuous two-particle wavefunction in real space. The Coulomb interaction V_c is included as

$$V_c = \sum_{n,m=1}^N V_{nm} |n, m\rangle \langle n, m| \quad (6)$$

The matrix elements are given by

$$\langle k, l | V_c | n, m \rangle = -\frac{e^2}{4\pi\epsilon_0\epsilon_r} \frac{\delta_{(n-m), (k-l)}}{|z_n - z_m| + \delta_r}, \quad (7)$$

where the small regularization constant δ_r avoids divergence at $z_n = z_m$, and $\delta_{(n-m), (k-l)}$ is the Kronecker delta ensuring translation invariance. This formulation inherently includes both short-range and long-range Coulomb correlations. The short-range contribution corresponds to the case $k = n$ and $l = m$, while long-range interactions are additionally accounted for by the off-diagonal terms where $n \neq m$. Figure 2 shows the matrix representation of the potential with the left subfigure 2 a) illustrating the short-range approximation, where only diagonal elements are retained. The right subfigure 2 b) includes the full long-range interaction, yielding a smoother and more physically accurate description of the electron-hole attraction over extended distances. In our model, we choose $\delta_r = a$, corresponding to the finite spatial extent of a lattice site.

III. EXAMPLES

A GeSn quantum well structure is investigated in the stationary regime using the proposed approach. The quantum well and the surrounding barriers are chosen to be of equal width, each consisting of 18 atoms aligned along the growth direction, which corresponds to approximately 10 nm. To study compositional effects, GeSn semiconductor structures with varying Sn concentrations of 8%, 9%, 10%, 11%, and 12% are considered. The relevant material parameters for these compositions, such as lattice constant, band gap energy, and electric permittivity, are estimated by extrapolation from

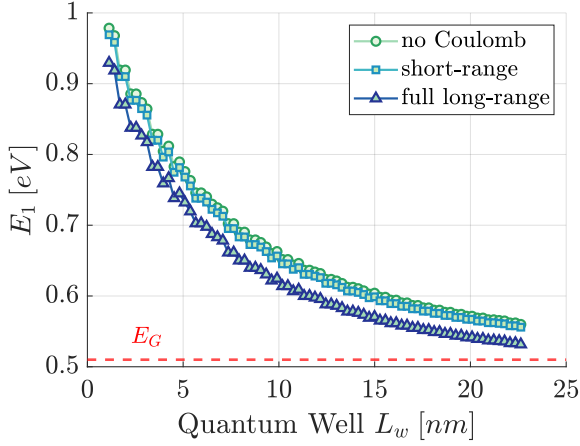


Fig. 3: Ground-state exciton energy E_1 as a function of the well width L_w in GeSn quantum wells. Coulomb effects dominate in narrow wells, reducing E_1 . The Sn concentration in this example is 8%. Reference: bulk bandgap energy E_G

available data for pure Ge and Sn [7]. This is done using Vegard's law [7], extended by a bowing parameter b_{GeSn} to account for nonlinear alloy mixing x

$$X_{Ge_{1-x}Sn_x}(x) = (1-x)X_{Ge} + xX_{Sn} - x(1-x)b_{GeSn} \quad (8)$$

where X represents a composition-dependent material parameter such as the band gap energy E_{gap} or lattice constant a , and b_{GeSn} is the bowing parameter that introduces a second-order correction to the otherwise linear interpolation. The bowing parameter has a critical impact on the electronic properties, as it captures the non-linear variation of key material properties, such as the band gap with increasing Sn content. Reported values vary widely between approximately 3.9 eV and 19 eV, introducing significant uncertainty in the electronic properties [8].

TABLE I: Material parameters for GeSn alloys with varying Sn content.

Sn (%)	8	9	10	11	12
E_{gap} (eV)	0.56	0.54	0.52	0.51	0.5
m_e	0.038	0.036	0.034	0.032	0.030
m_{hh}	0.18	0.17	0.16	0.15	0.14
a (nm)	0.5658	0.5662	0.5666	0.567	0.5674
ϵ_r	17.5	17.9	18.2	18.6	19

The material parameters used in this work are listed in Table I. Here, m_e and m_{hh} denote the effective masses of electrons and heavy holes, respectively, in units of the free electron mass. The parameter ϵ_r is the relative dielectric constant used for modeling Coulomb interaction and screening effects.

As illustrated in Figs. 3 and 4, the results show a clear dependence of the exciton ground-state energy E_1 on the quantum well width L_w and the Sn concentration. Coulomb effects, particularly the inclusion of long-range interactions,

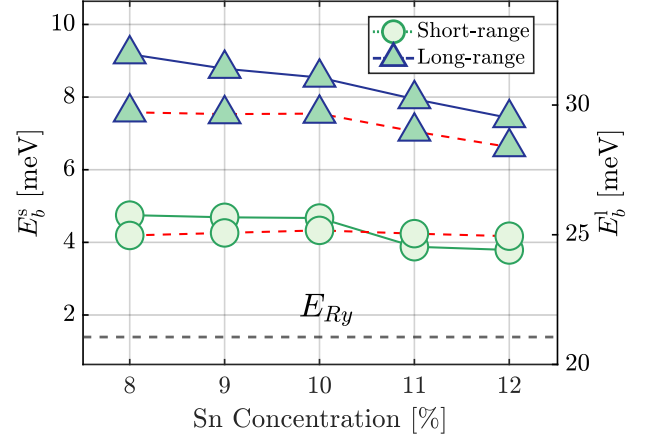


Fig. 4: Field-modified binding energies (5 mV/nm, red dashed) for different Sn concentrations. The binding energies E_b^s and E_b^l correspond to the short-range and long-range Coulomb interactions, respectively. Reference: Rydberg energy E_{Ry} .

lead to a pronounced redshift of E_1 , especially in narrow wells. As expected and shown in Fig. 4, the exciton binding energy E_b decreases with stronger Sn concentration and remains significantly above the bulk Rydberg limit E_{Ry} , even in the presence of an external electric field. The inclusion of the full long-range Coulomb interaction results in systematically larger exciton binding energies (~ 25 -35 meV), in contrast to only ~ 3 -6 meV obtained with short-range Coulomb interaction.

The corresponding excitonic absorption spectra are shown in Figs. 5 and 6, illustrating the impact of Sn concentration and external electric fields, respectively. To compute the absorption spectra, we calculate the imaginary part of the optical susceptibility, since it directly relates to the absorption strength. A Lorentzian lineshape is used to model the finite linewidth of each transition. The total absorption coefficient is then obtained by summing over all individual excitonic transitions

$$\alpha(\omega) \propto \text{Im} \chi(\omega) \propto \sum_n M_n \cdot \frac{\gamma/\pi}{(\omega - E_n)^2 + \gamma^2} \quad (9)$$

where E_n denotes the energy of the n -th bound exciton state, M_n its corresponding oscillator strength, and γ is the phenomenological parameter accounting for homogeneous lifetime broadening. This approach enables a direct link between the discrete excitonic eigenstates obtained from the solution of the interacting Hamiltonian and their spectroscopic signature. In the present model, only the excitonic ground state significantly contributes to the absorption spectrum, resulting in a single dominant peak. Higher-lying states are either optically inactive or contribute negligibly due to their reduced oscillator strength.

Figure 5 compares the absorption spectra for various Sn concentrations, contrasting the short-range and long-range Coulomb models. With increasing Sn content (from 8% to 12%), a systematic redshift of the absorption peak is observed, reflecting the reduced confinement and smaller bandgap in the well material. This redshift is significantly more pronounced

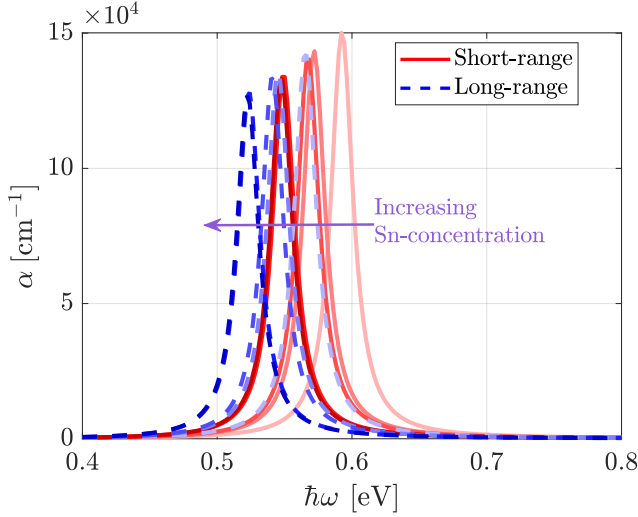


Fig. 5: Ground-state excitonic absorption spectra $\alpha(\omega)$ for different Sn concentrations, comparing short- (red lines) and long-range (blue dashed) Coulomb interactions. An increasing Sn-concentration (up to 12%) results in a redshift.

in the full long-range Coulomb treatment, which accounts for the extended electron-hole attraction across the entire heterostructure. In contrast, the short-range model, based only on diagonal Coulomb terms, underestimates the attractive interaction, resulting in higher excitonic resonance energies.

Moreover, the long-range model leads to broader and less intense absorption peaks. This reduction in peak amplitude can be attributed to the larger spatial extent of the exciton wavefunction, which lowers the overlap between electron and hole wavefunctions and thus reduces the oscillator strength M_n . The short-range approximation yields more localized excitons with larger oscillator strengths and, consequently, sharper spectral features.

Figure 6 presents the field-dependent absorption spectra for a fixed Sn concentration. Here, we observe a characteristic redshift (Stark shift) of the excitonic resonance with increasing electric field strength. This effect is again more pronounced in the long-range model, consistent with the stronger field-induced spatial separation of electron and hole components. The asymmetric distortion of the excitonic wavefunction under the external field leads not only to a reduction of binding energy but also to a further suppression of oscillator strength, resulting in a broader and weaker absorption signal.

IV. DISCUSSION AND CONCLUSION

Our stationary treatment provides detailed insight into the bound exciton states in GeSn quantum wells and highlights how the potential shape and interaction range affect the resulting energy levels and optical response. We find that including the full long-range Coulomb interaction significantly increases the exciton binding energy (up to ~ 35 meV compared to ~ 5 meV in the short-range model) and induces a noticeable redshift in the absorption spectrum. The spectra are

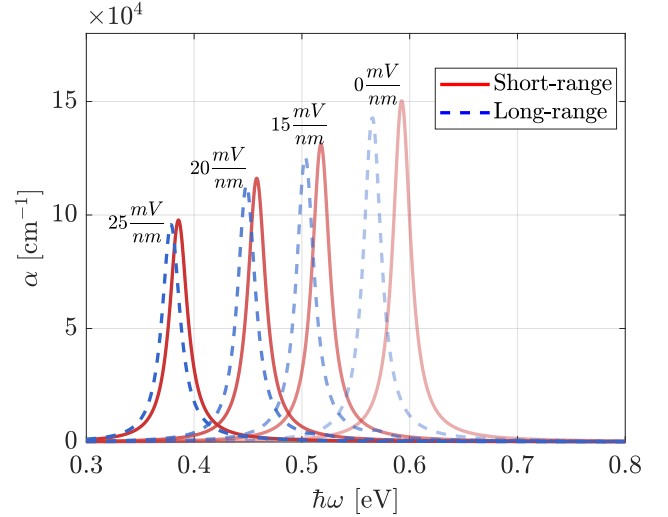


Fig. 6: Ground-state excitonic absorption spectra $\alpha(\omega)$ under varying electric fields, comparing short- and long-range Coulomb interactions. An increasing field strength results in a Stark shift.

consistently dominated by the excitonic ground state, which carries nearly the entire oscillator strength. Variations in Sn concentration directly influence both the dielectric screening and quantum confinement, with higher Sn contents enhancing exciton localization and binding. External electric fields lead to Stark shifts in the absorption spectrum, consistent with the field-induced spatial separation of the electron-hole pair.

Future work could extend the presented framework by including a light-matter interaction term H_{em} in the Hamiltonian, as well as strain effects, non-parabolic band structures, or time-dependent excitation scenarios to further explore and optimize GeSn-based optoelectronic devices.

REFERENCES

- [1] Liu, M., Junk, Y., Han, Y. et al. *Vertical GeSn nanowire MOSFETs for CMOS beyond silicon.*, Commun Eng **2**, 7 (2023).
- [2] Z. Hens, Christophe Delerue. *A Tight-Binding Model for Illustrating Exciton Confinement in Semiconductor Nanocrystals.*, The Journal of Chemical Physics, 2024, 160 (11), pp.114106.
- [3] Abdi, A. and Schulz, D. *Application of the tight-binding method onto the Von Neumann equation*, J Comput Electron **23**, 707–717 (2024).
- [4] Huhn, W. and Stahl, A. *Self-Consistent Field Theory Applied to the Semiconductor Band Edge*, phys. stat. sol. **124**, **167**, 167-179 (1984).
- [5] Peschel, U., Thümmel, M., Lettau, T., Gräfe, S. and Busch, K. *Two-particle tight-binding description of higher-harmonic generation in semiconductor nanostructures*, Phys. Rev. B **106**, 24 (2022).
- [6] Mukhopadhyay, B., Sen, G., Chang, G. E. and Basu, P.K. *Exciton Binding Energy in $Ge_{1-x}Sn_x$ Quantum Wells: Fractional Dimensional and k.p Calculations*, URSI AP-RASC (2019).
- [7] Moontragoon, P., Soref, R. A. and Ikonik, Z. *The direct and indirect bandgaps of unstrained $Si_xGe_{1-x-y}Sn_y$ and their photonic device applications*, J. Appl. Phys. **112**, 7 (2012).
- [8] Stange, D. et al. *Short-wave infrared LEDs from GeSn/SiGeSn multiple quantum wells*, Optica **4**, 185-188 (2017).